Int. J. Electrochem. Sci., 8 **(2013)** 2945 - 2957

International Journal of ELECTROCHEMICAL SCIENCE
www.electrochemsci.org

Hydrated Cobalt Nickel Molybdate Nanorods as Effectively Supercapacitor Electrode Materials

Yuanying Liu[1], Huan Pang[1, 2, 3,], Jinfu Guo[1], Weiqiang Wang[1], Zhenzhen Yan[1], Le Ma[1], Yahui Ma[1], Guochang Li[1], Jing Chen[1],*[*] *Jiangshan Zhang[1] and Honghe Zheng[2*]*

[1] College of Chemistry and Chemical Engineering, Anyang Normal University, Anyang, 455000, Henan, P. R. China.
[2] School of Energy, Soochow University, Suzhou, 215006, Jiangsu, P. R. China.
[3] State Key Laboratory of Coordination Chemistry, Nanjing University, Nanjing, 210093, Jiangsu, P. R. China.
[*]E-mail: huanpangchem@hotmail.com; chenjing64@eyou.com; hhzheng@suda.edu.cn

Received: 28 November 2012 / *Accepted:* 30 December 2012 / *Published:* 1 February 2013

One-dimensional $Co_xNi_{1-x}MoO_4 \cdot nH_2O$ ($0 \le x \le 1$) nanorods have been successfully synthesized by a mild hydrothermal method. The chemical composition of nanorods was varied. Structures and morphologies of samples were characterized by X-ray diffraction (XRD), field-emission scanning electron microscope (FE-SEM), and the specific surface area of samples has also been studied by using the Brunauer-Emmet-Teller isotherm. More importantly, the supercapacitive performances of $Co_xNi_{1-x}MoO_4 \cdot nH_2O$ nanorods were also studied by using cyclic voltammetry, galvanostatic charge/discharge measurements, and electrochemical impedance spectroscopy (EIS) methods in 1.0 M KOH solution. The electrochemical measurements showed that $Co_xNi_{1-x}MoO_4 \cdot nH_2O$ electrodes exhibited good supercapacitive activity in KOH electrolyte. The specific capacitance has been effected by the ratio of Co/Ni, when the x value is 0.5, the specific capacitance of $Co_{0.5}Ni_{0.5}MoO_4 \cdot nH_2O$ electrode can achieve the largest one, 1040.7 F g^{-1} at the current density of 0.625 A g^{-1} under our experiment condition, and after 400 charge-discharge cycles at 0.625 A g^{-1} the specific capacitance of $Co_{0.5}Ni_{0.5}MoO_4 \cdot nH_2O$ electrode has maintained 98.3 % of the initial value. This enhanced electrochemical performance of $Co_{0.5}Ni_{0.5}MoO_4nH_2O$ nanorods might be ascribed to efficient surface area and electron transport path, which were facilitated by one-dimensional nanostructure.

Keywords: Cobalt nickel molybdate; nanorods; supercapacitor electrode materials

1. INTRODUCTION

Recently, shape-controlled synthesis of low-dimensional nanocrystals has been an intense focus of the research in nanotechnology for their unique physical and chemical properties, and their potential technological applications [1-7]. The synthesized nanomaterials have been an important and hot

research top in the electrochemical capacitors because of their high surface area-to-volume ratio, less agglomerated configuration, shortened diffusion paths and fast redox reactions in the solid phase [8-10]. Nanorods, one of the one-dimensional nanostructures, are ideal building blocks for nanoscale electronics, optoelectronics, and sensing devices, meanwhile they represent large surface area, short distance for mass and charge transport, and freedom for volume change [11-18]. Normally, the electrical conductivity of electrode materials is one of the most important respects in mitigating the internal resistance of the capacitors and enhancing the utilization of active materials [19]. Thus the synthesis of one-dimensional nanostructures to be used in the field of electrode materials is highly desirable for materials researchers [20-26].

With the increasing demand of high power portable electronic devices and electric vehicles, electrochemical capacitors that deliver higher power density than traditional batteries have been studied extensively in recent years [27–31]. In particular, hydrous ruthenium oxides based materials exhibit much outstanding specific capacitance, longer cycle life than conventional materials. However, the high cost of this noble metal material limits it from commercialization and searching for alternative inexpensive electrode materials is indispensable.

Metal molybdate, $AMoO_4$-type compounds (where A is a divalent metal ion), are an interesting research topic due to their potential application in many fields, such as: magnetic properties, photoluminescence, and catalysts [32-40]. Mai et al. group [35] has successfully synthesized the three-dimensional multi-component oxide, $MnMoO_4/CoMoO_4$ and fabricated asymmetric supercapacitors based on hierarchical $MnMoO_4/CoMoO_4$ heterostructured nanowires. Kong et al. group [36] has successfully reported that $CoMoO_4$ $0.9H_2O$ nanorods were fabricated by a hydrothermal method and its excellent electrochemical capacitive behavior was demonstrated. However, there are little reports about the electrochemical supercapacitor of $Co_xNi_{1-x}MoO_4{\cdot}nH_2O$ composite nanomaterial.

In this work, we have successfully synthesized $Co_xNi_{1-x}MoO_4{\cdot}nH_2O$ ($0 \le x \le 1$) nanorods by the modified method of Kim et al. group [25]. The electrochemical properties of $Co_xNi_{1-x}MoO_4{\cdot}nH_2O$ ($0 \le x \le 1$) nanorods were studied systematically as electrochemical capacitor electrodes. We also discovered that different chemical compositions have a remarkable effect on the capacitive behavior of the samples. The electrochemical measurements showed that $Co_xNi_{1-x}MoO_4{\cdot}nH_2O$ electrodes exhibit good supercapacitive characteristics in 1.0 M KOH electrolyte. The specific capacitance has been effected by ratio of Co/Ni, when the x value is 0.5, the specific capacitance of $Co_{0.5}Ni_{0.5}MoO_4{\cdot}nH_2O$ electrode can achieve at 1040.7 F g^{-1} at the current density of 0.625 A g^{-1} under our experiment conditions, and after 400 charge-discharge cycles at 0.625 A g^{-1} the specific capacitance of $Co_{0.5}Ni_{0.5}MoO_4{\cdot}nH_2O$ electrode have maintained 98.3 % of the initial value. This enhanced electrochemical performance of $Co_{0.5}Ni_{0.5}MoO_4nH_2O$ nanorods might be ascribed to their large surface area and efficient electron transport path, which were facilitated by one-dimensional nanostructure.

2. EXPERIMENTAL

2.1 Materials and preparation

Analytical grade $Co(NO_3)_2 \cdot 6H_2O$ (Aladdin Chemistry Co., Ltd), $Ni(NO_3)_2 \cdot 6H_2O$ (Guangfu Technology Development Co., Ltd, Tianjin, China), $Na_2MoO_4 \cdot 2H_2O$ (Taizhou Chemical Plant, Guangdong, China) were used as source materials.

$Co_xNi_{1-x}MoO_4.nH_2O$ nanorods have been synthesized by a simple hydrothermal precipitation without using any structure directing agents. In a typical procedure, to prepare solutions (total molar concentration of 0.05 mol L^{-1}) with a molar fraction (x) of Co (x =0, 0.25, 0.5, 0.75, and 1), controlled amounts of Ni- and Co- containing reagents were dissolved in 16 mL deionized water under constant magnetic stirring, then 0.8 mmol $Na_2MoO_4 \cdot 2H_2O$ was added into the solution. This resulting solution was transferred into a Teflon-lined stainless steel autoclave, sealed and maintained at 180 °C for 8 h, then allowed to cool room temperature naturally. After that the resulting white solid products obtained at the bottom of the autoclave were collected by centrifugation, washed with deionized water and absolute alcohol several times, and then dried in air before further characterization.

2.2 Characterization

X-ray powder diffraction patterns (XRD) of the products were recorded by a D8 diffractometer in the 2θ range of 10-70^o by using a Japan Rigaku Ultima III X-ray diffractometer with graphite monochromatized Cu Kα radiation (λ= 1.5418 Å). The field-emission scanning electron microscope (FE-SEM) measurements were carried out with a field-emission microscope (JEOL 6701F equipped with a Bruker EDX detector) at an acceleration voltage of 5.0 KV. Nitrogen adsorption-desorption measurements were performed on a Gemini VII 2390 Analyzer at 77.0 K with the volumetric method. The specific surface area was obtained from the N_2 adsorption-desorption isotherms and was calculated by the Brunauer-Emmett-Teller (BET) method.

2.3 Electrochemical experiments

Electrochemical study on $Co_xNi_{1-x}MoO_4.nH_2O$ electrodes was carried out on a CHI- 660D electrochemical workstation (Chenhua CHInstrument, Inc.). All electrochemical performances were carried out in a conventional three-electrode system equipped with platinum foil as a counter electrode, and all potentials in this work were referred to a saturated calomel electrode (SCE) reference electrode. The working electrode was made from mixing of $Co_xNi_{1-x}MoO_4.nH_2O$ as active materials, acetylene black, and PTFE (polytetrafluoroethylene) with a weight ratio of 85:15:5, coating on a piece of foamed nickel of the area within 1 cm^2, and pressing to be a thin foil at a pressure of 5 MPa. 1.0 mol L^{-1} KOH solution was served as the electrolyte at room temperature. Cyclic voltammetry (CV) was performed at various scan rates of 5, 10, 20, 30, 50 and 100 mV s^{-1}. Galvanostatic (GV) charge/discharge curves were obtained at various current densities of 0.625, 1.25, 2.50, 3.75 and 6.25 A g^{-1} to evaluate the specific capacitance. A potential window in the range from 0 to 0.45 V was used in all measurements.

And electrochemical impedance spectroscopy (EIS) measurements were conducted at open circuit voltage in the frequency range of 100 kHz to 0.01 Hz with AC voltage amplitude of 5 mV using PARSTAT 2273.

3. RESULTS AND DISCUSSIONS

3.1 Crystal structure, EDS microanalysis and morphology of as-synthesized $Co_xNi_{1-x}MoO_4 \cdot nH_2O$

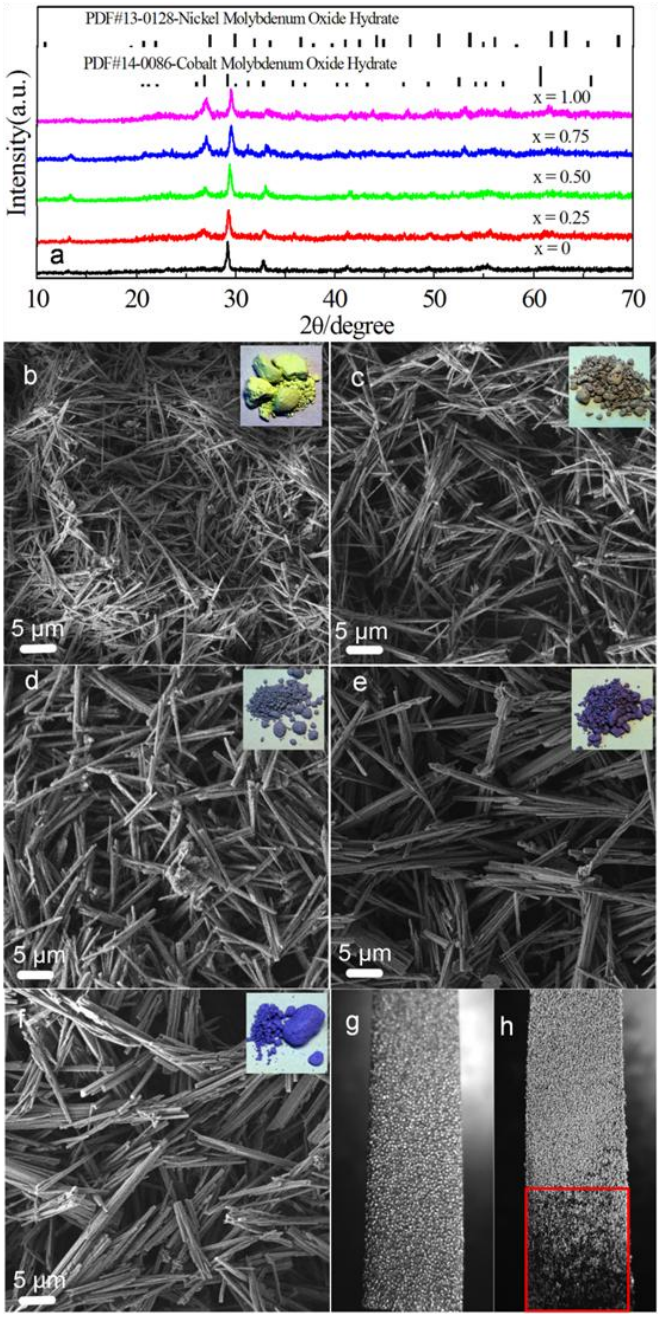

Figure 1. (a) X-ray diffraction patterns of as-synthesized $Co_xNi_{1-x}MoO_4 \cdot nH_2O$ nanorods with various x values; (b-f) their corresponding typical FE-SEM images, in inset of b-f optical photos of $Co_xNi_{1-x}MoO_4 \cdot nH_2O$ nanorods; (g) pure Ni foam; (h) Ni foam modified activated materials.

The crystalline structures of the as-synthesized $Co_xNi_{1-x}MoO_4 \cdot nH_2O$ nanorods were confirmed by their XRD patterns in Fig. 1a. When the value of x was 0, the diffraction peaks at 2θ = 27.3 and 29.9 could be indexed as $NiMoO_4 \cdot nH_2O$ (JCPDS card No.13-0128). When the value of x was 1, the diffraction peaks at 2θ = 29.9 and 33.4 could be indexed as $CoMoO_4 \cdot nH_2O$ (JCPDS card No.26-0477). When the values of x changed from 0.25 to 0.75, the diffraction peak at 2θ = 27.3 weakened, and the diffraction peak at 2θ = 33.4 gradually enhanced. In inset of Fig. 1, there are corresponding optical images of samples, and the color of samples has changed from yellow to blue as the increasing of Co.

The corresponding EDS mappings of $Co_xNi_{1-x}MoO_4 \cdot nH_2O$ nanorods were also tested (ESI Fig. 1–5) to further confirm the ratio of Co and Ni elements. And from images of ESI Fig. 1-5, we can see that there are four color mapping images, which are green –Ni-K, purple-Mo-L, red-O-K and blue-Co-K respectively. As the reduction of element content, the color has faded, and it is clear that the green-Ni-K image has faded as the decreasing of Ni and blue-Co-K image has being strong as increasing of Co. Quantitative analysis of ratio of Co and Ni elements was also tested, which further confirmed X= 0, 0.25, 0.50, 0.75 and 1.00, respectively.

Table 1. Brunauer-Emmett-Teller (BET) measurements of samples

X value	Surface area ($m^2\ g^{-1}$)
0	40.6
0.25	22.2
0.5	12
0.75	8.2
1	7.8

The size and morphology of as-synthesized $Co_xNi_{1-x}MoO_4 \cdot nH_2O$ with various cationic compositions were examined by field emission scanning electron microscopy (FE-SEM). Fig. 1b-f shows typical FE-SEM images of as-synthesized $Co_xNi_{1-x}MoO_4 \cdot nH_2O$. It indicates that all of the samples almost completely consist of nanorod structures despite of their different ratios of Co/Ni. However, the aspect ratio of nanorods tended to decrease with increasing the concentration of Co, which could lead to a decreasing in their surface area. To confirm the change in surface area that may have occurred during changing the composition of $Co_xNi_{1-x}MoO_4 \cdot nH_2O$ nanorods, Brunauer-Emmett-Teller (BET) method was carried out at liquid nitrogen temperature. From the results presented in Table 1, it is confirmed that the surface area of $Co_xNi_{1-x}MoO_4 \cdot nH_2O$ nanorods gradually decreased as increasing Co concentration because of the corresponding decreasing of aspect ratio. In Fig. 1g, there is a piece of pure Ni foam, which is used to prepare work electrode seen in Fig. 1h. The red box area is activated material area.

Recently, most reports have been focused on the lithium reactivity of molybdates because they could deliver high reversible capacity through a conversion reaction with lithium [25, 38]. In this work, we have successfully studied electrochemical supercapacitor properties of $Co_xNi_{1-x}MoO_4 \cdot nH_2O$ nanorods. To evaluate the electrochemical capacitive performance of $Co_xNi_{1-x}MoO_4 \cdot nH_2O$ nanorod electrode, typical cyclic voltammetry experiments were firstly recorded at scan rates of 5, 10, 20, 30,

50, 100 mV s^{-1} within potential windows ranging from 0 to 0.45 V in 1.0 mol L^{-1} KOH electrolytes at room temperature. Fig. 2a shows the CV curves of $Co_xNi_{1-x}MoO_4 \cdot nH_2O$ nanorod electrodes at a scan rate of 5 mV s^{-1}, and the shapes of the CV curves reveal that they all have big surrounded areas, indicating that the capacitance mainly results from the pseudo capacitive capacitance, especially for that of $Co_{0.5}Ni_{0.5}MoO_4 \cdot nH_2O$. Specific capacitances derived from cyclic voltammetry (CV) tests can be calculated from the following equation [41]:

$$C = \frac{1}{m\upsilon(V_c - V_a)} \int_{V_a}^{V_c} I(V)dV \quad (1)$$

where C (F g^{-1}), m (g), υ (mV s^{-1}), V_c and V_a, and I (A) are the specific capacitance, the mass of active materials in the electrode, potential scan rate, high and low potential limit of the CV tests, and the instant current on CV curves, respectively.

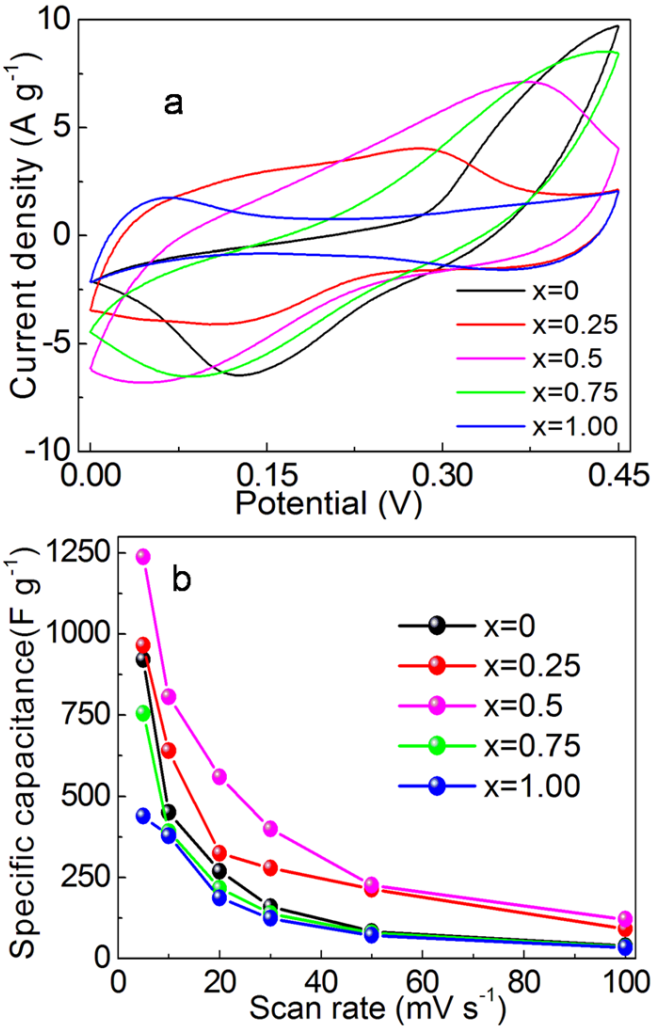

Figure 2. (a) CV curves of $Co_xNi_{1-x}MoO_4 \, nH_2O$ nanorods electrodes at a scan rate of 5 mV s^{-1}; (b) the specific capacitances calculated from CV curves at the scan rates of 5-100 mV s^{-1}.

The specific capacitances calculated from the CV curves at the scan rates of 5-100 mV s^{-1} are shown in Fig. 2b. When the values of x were 0, 0.25, 0.5, 0.75 and 1, the specific capacitance of $Co_xNi_{1-x}MoO_4 \cdot nH_2O$ nanorod electrodes at the scan rate of 5 mV s^{-1} can achieve 920.3 F g^{-1}, 965.0 F g^{-1}, 1237.5F g^{-1}, 755.5 F g^{-1} and 439.7 F g^{-1}, respectively. It clearly reveals that the $Co_xNi_{1-x}MoO_4 \cdot nH_2O$ nanorod electrode with x value of 0.5 has the largest specific capacitance which indicates that it has good electrochemical capacitive properties.

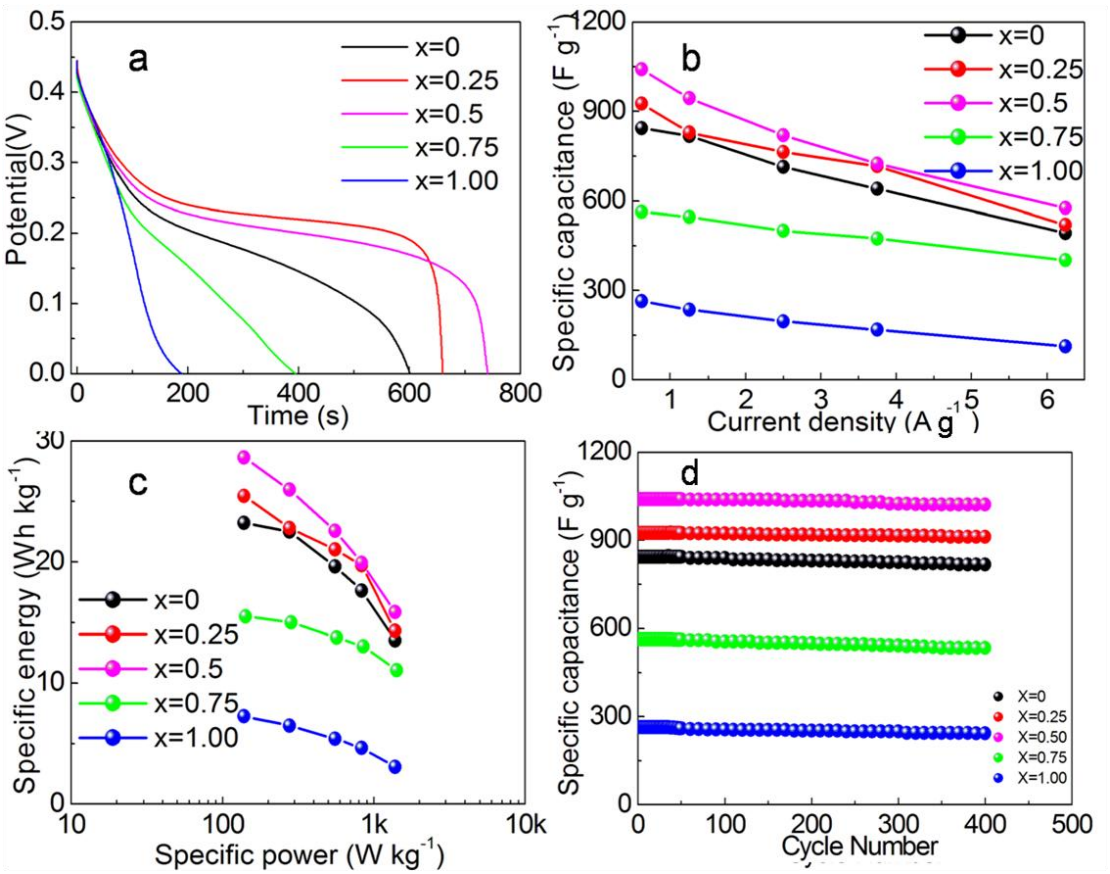

Figure 3. (a) the galvanostatic discharge curves of the as-prepared $Co_xNi_{1-x}MoO_4\ nH_2O$ nanorods at the current densities of 0.625 A g^{-1}; (b) the specific capacitances derived from discharging curves at the current density of 0.625-6.25 A g^{-1}; (c) the relationship of specific energy against specific power for five samples; (d) the relationships of the specific capacitance against cycling number for five samples with current density 0.625 A g^{-1}.

Good rate capability is an important requirement of supercapacitors. To further investigate the electrochemical performances of $Co_xNi_{1-x}MoO_4 \cdot nH_2O$ nanorod electrodes, galvanostatic charge/discharge measurements were carried out in the potential range 0-0.45 V at various current densities of 0.625, 1.25, 2.50, 3.75 and 6.25 A g^{-1}. The galvanostatic discharge curves of the as-prepared $Co_xNi_{1-x}MoO_4 \cdot nH_2O$ nanorod at the current density of 0.625 A g^{-1} are shown in Fig. 3a. The specific capacitance of an electrode during galvanostatic charge/discharge can be calculated by the following equation [41]:

$$C = \frac{i \cdot \Delta t}{m \cdot \Delta V} \quad (2)$$

Where m is the mass of $Co_xNi_{1-x}MoO_4 \cdot nH_2O$ (g), ΔV is the range of the charge/discharge (V), and i is the discharge current (A) applied for time Δt (s). The specific capacitances derived from the discharging curves at the current density of 0.625-6.25 A g^{-1} are shown in Fig. 3b. When the values of x were 0, 0.25, 0.5, 0.75 and 1, the specific capacitance of $Co_xNi_{1-x}MoO_4 \cdot nH_2O$ nanorod electrodes at the current density of 0.625 A g^{-1} were calculated to be 844.1 F g^{-1}, 925.6 F g^{-1}, 1040.7 F g^{-1}, 563.2 F g^{-1} and 264.0 F g^{-1}, respectively. Specific energy and specific power are two key factors for evaluating the power applications of electrochemical supercapacitors. A good electrochemical supercapacitor is expected to both provide high energy density and powder density. Specific energy (E) and specific power (P) derived from GV tests can be calculated from the following equations [41]:

$$E = \frac{1}{2} C \Delta V^2 \quad (3)$$

$$P = \frac{E}{\Delta t} \quad (4)$$

Where E (Wh kg^{-1}), C (F g^{-1}), ΔV (V), P (W kg^{-1}) and Δt (s) are the specific energy, specific capacitance, the range of the charge/discharge (V), specific power and discharge time, respectively. Fig. 3c shows Ragone plot for $Co_xNi_{1-x}MoO_4 \cdot nH_2O$ nanorod electrodes at the potential window of 0.45 V in 1.0 mol L^{-1} KOH aqueous solution.

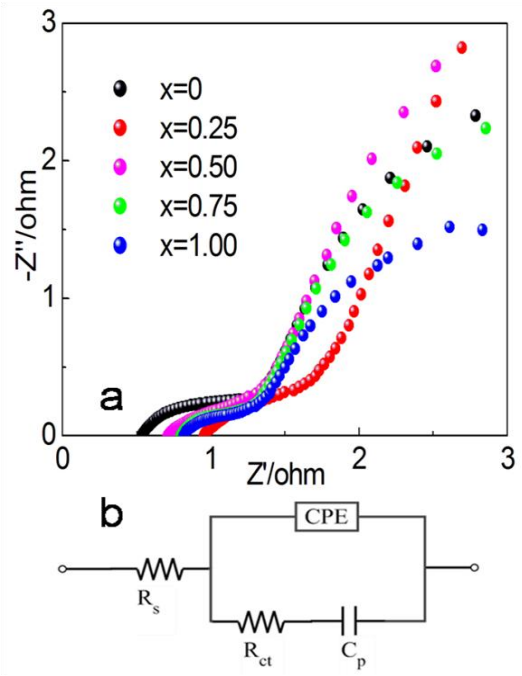

Figure 4. (a) the electrochemical impedance spectra of the electrodes at room temperature; (b) the equivalent circuit for the electrochemical impedance spectrum.

When the value of x was 0.5, the specific energy of $Co_{0.5}Ni_{0.5}MoO_4 \cdot nH_2O$ decreased from 28.6 to 15.8 Wh kg^{-1}, while the specific power increased from 139.1 to 1387.6 W kg^{-1} as the galvanostatic (GV) charge/discharge current increased from 0.625 to 6.25 A g^{-1}. The variation of specific capacitance as a function of cycle number is shown in Fig. 3d at 250 $mA \cdot g^{-1}$, and reveals that all $Co_xNi_{1-x}MoO_4 \cdot nH_2O$ materials electrodes have good recycle properties for electrochemical capacitors, especially for $Co_{0.5}Ni_{0.5}MoO_4 \cdot nH_2O$. It is only approximately 0.1% loss of specific capacitance after 100 cycles and 1.7 % loss even after 400 cycles, which might be caused by the decomposition of micro/nanostructures. Compared with it, specific capacitance of $CoMoO_4 \cdot nH_2O$ materials electrode can be maintained 92.0% after 400 cycles.

The electrode kinetics of the as-prepared material electrodes was estimated by electrochemical impedance spectra. The electrochemical impedance spectra analyses of $Co_xNi_{1-x}MoO_4 \cdot nH_2O$ nanorod electrodes were measured at room temperature in the frequency range 10^{-3}–10^6 Hz in the same setup as the CV and GV tests and the corresponding Nyquist plots in the typical form of Nyquist plots (Z' vs. Z") is shown in Fig. 4a. In general, the impedance curves present two partially overlapped semicircles in the high- and medium-frequency regions and an inclined line in the low-frequency region. An equivalent circuit used to fit the impedance curve is given in Fig. 4b, which is similar to the circuit employed for the working electrode of supercapacitor. The electrochemical impedance spectra data can be fitted by a bulk solution resistance R_s, a charge-transfer R_{ct} and a pseudocapacitive element C_p from redox process of $Co_xNi_{1-x}MoO_4 \cdot nH_2O$, and a constant phase element (CPE) to account for the double-layer capacitance. The solution resistance R_s of these five composites was measured to be 0.53, 0.95, 0.71, 0.80 and 0.82 Ω, respectively, while the charge-transfer resistance R_{ct} was calculated (by ZSimpWin software) to be 15.9, 11.2, 5.5, 17.8 and 27.9 Ω, respectively. This clearly demonstrates the reduced charge-transfer resistance of the $Co_{0.5}Ni_{0.5}MoO_4 \cdot nH_2O$ nanorods electrode. In addition, the charge-transfer resistance R_{ct}, also called Faraday resistance, is a limiting factor for the specific power of the supercapacitor. It is the low Faraday resistance that results in the high specific power of the $Co_{0.5}Ni_{0.5}MoO_4 \cdot nH_2O$ nanorods electrode. The charge-transfer resistance R_{ct} of the $Co_{0.5}Ni_{0.5}MoO_4 \cdot nH_2O$ nanorods electrode is the lowest of all, which makes high electric activity.

4. CONCLUSIONS

In summary, we have successfully synthesized $Co_xNi_{1-x}MoO_4 \cdot nH_2O$ ($0 \leq x \leq 1$) nanorods through a facile hydrothermal method without the assistance of surfactants and templates. The x value has a great influence on the specific surface areas of the samples. The measurement of electrochemical supercapacitor properties of $Co_xNi_{1-x}MoO_4 \cdot nH_2O$ materials is an important work. We found that different chemical composition had a remarkable effect on the electrochemical properties. When the x value was 0.5, the specific capacitance of $Co_xNi_{1-x}MoO_4 \cdot nH_2O$ electrode could achieve above 1000 F g^{-1}, which illustrates $Co_xNi_{1-x}MoO_4 \cdot nH_2O$ materials could be applied as an outstanding electroactive material for supercapacitor.

References

1. H. Pang, Q. Y. Lu, Y. Z. Zhang, Y. C. Li, F. Gao, *Nanoscale* 2 (2010) 920.
2. H. Pang, J.W. Deng, B. Yan, Y. H. Ma, G. C. Li, Y. N.Ai, J. Chen, J. S. Zhang, H. H. Zheng, J. M. Du, *Int. J. Electrochem. Sci*. 7 (2012) 10735.
3. H. Pang, Z. Z. Yan, W. Q. Wang, Y. Y. Wei, X. X. Li, J. Li, J. Chen, J. S. Zhang, H. H. Zheng, *Int. J. Electrochem. Sci*. 2012 accepted.
4. K. B. Zhou, X. Wang, X. M. Sun, Q. Peng, Y. D. Li, *J. Catal.* 229 (2005) 206
5. C. Burda, X. Chen, R. Narayanan, M. A. El-Sayed, *Chem. Rev.* 105 (2005) 1025
6. T. Ghoshal, S. Biswas, S. Kar, *J. Phys. Chem. C.* 112 (2008) 20138
7. S. Acharya, A. B. Panda, S. Efrimaa, Y. Golan, *Adv. Mater.* 19 (2007) 1105
8. S. Acharya, I. Patla, J. Kost, S. Efrima, Y. Golan, *J. Am. Chem. Soc.* 128 (2006) 9294
9. D. D. Zhao, M. W. Xu, W. J. Zhou, J. Zhang, H. L. Li, *Electrochim. Acta* 53 (2008) 2699
10. S. L. Xiong, C. Z. Yuan, X. G. Zhang, B. J. Xi, Y. T. Qian, *Chem.–Eur. J.* 15 (2009) 5320
11. Y. G. Wang, Y. Y. Xia, *Electrochim. Acta* 51(2006) 3223
12. S. Kar, S. Santra, S. Chaudhuri, *Cryst. Growth Des.* 8 (2008) 344
13. S. Kar, S. Santra, H. Heinrich, *J. Phys. Chem. C.* 112 (2008) 4036
14. Y. Huang, X. F. Duan, Y. Cui, L. J. Lauhon, K. H. Kim, C. M. Lieber, *Science* 294 (2001) 1313
15. C. Z. Wu, J. Dai, X. D. Zhang, J. L. Yang, Y. Xie, *J. Am. Chem. Soc.* 131 (2009) 7218
16. C. N. R. Rao, F. L. Deepak, G. Gundiah, Prog. *Solid State Chem.* 31 (2003) 5
17. S. Kar, T. Ghoshal, S. Chaudhuri, *Chem. Phy. Lett.* 419 (2006) 174
18. Y. Wang, G. Z. Cao, *Adv. Mater.* 20 (2008) 2251
19. Y. G. Guo, J. S. Hu, L. J. Wan, *Adv. Mater.* 20 (2008) 2878
20. M. S. Wu, H. H. Hsieh, *Electrochimica. Acta* 53 (2008) 3427
21. W. Y. Li, L. N. Xu, J. Chen, *Adv. Funct. Mater.*15 (2005) 851
22. Y. G. Li, B. Tan, Y. Y. Wu, *J. Am. Chem. Soc.* 128 (2006) 14258
23. C. Z. Yuan, X. G. Zhang, L. H. Su, B. Gao, L. F. Shen, *J. Mater. Chem.*19 (2009) 5772.
24. C. Z. Yuan, B. Gao, X. G. Zhang, *J. Power Sources* 173 (2007) 606.
25. J. Jiang, J. P. Liu, X. T. Huang, Y. Y. Li, R. M. Ding, X. X. Ji, Y. Y. Hu, Q. B. Chi, Z. H. Zhu, *Cryst. Growth Des.* 10 (2010) 70.
26. K. S. Park, S. D. Seo, H. W. Shim, D. W. Kim, *Nanoscale Research Letters* 7 (2012) 35.
27. J. Liu, X. Huang, Y. Li, Z. Li, *J. Mater. Chem.* 17 (2007) 2754.
28. C. Liu, F. Li, L. P. Ma, H. M. Cheng, *Adv. Mater.* 22 (2010) E28.
29. P. Simon, Y. Gogotsi, *Nat. Mater.* 7 (2008) 845.
30. S. Chen, J. W. Zhu, X. D. Wu, Q. F. Han, X. Wang, *ACS Nano* 4 (2010) 2822.
31. V. Subramanian, H. W. Zhu, R. Vajtai, P. M. Ajayan, B. Q. Wei, *J. Phys. Chem. B* 109 (2005) 20207.
32. P. J. Hall, M. Mirzaeian, S. I. Fletcher, F. B. Sillars, A. J. R. Rennie, G. O. Shitta-Bey, G. Wilson, A. Cruden, R. Carter, *Energy Environ. Sci.* 3 (2010) 1238.
33. J. Rodriguez, S. Chaturvedi, J. Hanson, A. Albornoz, *J. Phys. Chem. B* 102 (1998) 1347.
34. W. G. Chu, H. F. Wang, Y. J. Guo, L. N. Zhang, Z. H. Han, *Inorg. Chem.* 48 (2009) 1243.
35. S. Vilminot, G. André, M. Kurmoo, *Inorg. Chem.* 48 (2009) 2687.
36. L. Q. Mai, F. Yang, Y. L. Zhao, X. Xu, L. Xu, Y. Z. Luo, *Nat. Commun.* 2 (2011) 381.
37. M. C. Liu, L. B. Kong, X. J. Ma, C. Lu, X. M. Li, Y. C. Luo and L. Kang, *New J. Chem.* (2012) doi 10.1039/c2nj40278e.
38. M. Bonanni, L. Spanhel, M. Lerch, E. Fuglein, G. Muller, *Chem. Mater.* 10 (1998) 304.
39. W. Xiao, J. S. Chen, C. M. Li, R. Xu, X. W. Lou, *Chem. Mater.* 22 (2010) 746.
40. Y. Ding, Y. Wan, Y. L. Min, W. Zhang, S. H. Yu, *Inorg. Chem.* 47 (2008) 7813.
41. S. J. Yang, Y. G. Liang, Z. H.Yi, X. L. Ma, J. T. Sun, *J. Alloys Compd.* 433 (2007) 324.
42. L. H. Bao, J. F. Zang, X. D. Li, *Nano Lett.* 10 (2010) 1021.

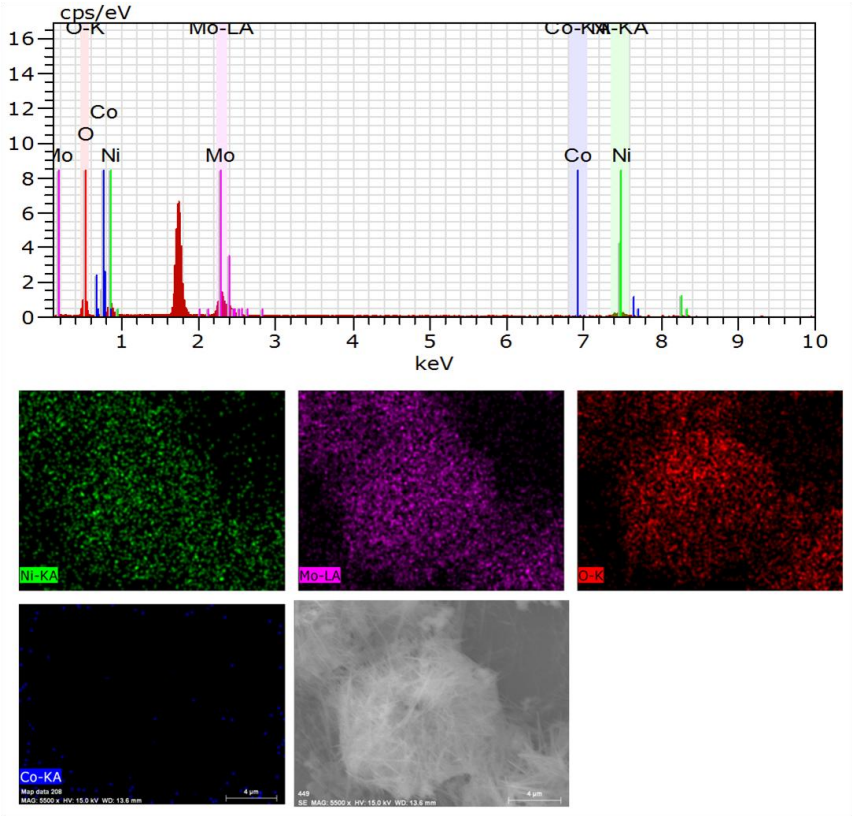

ESI Fig. 1

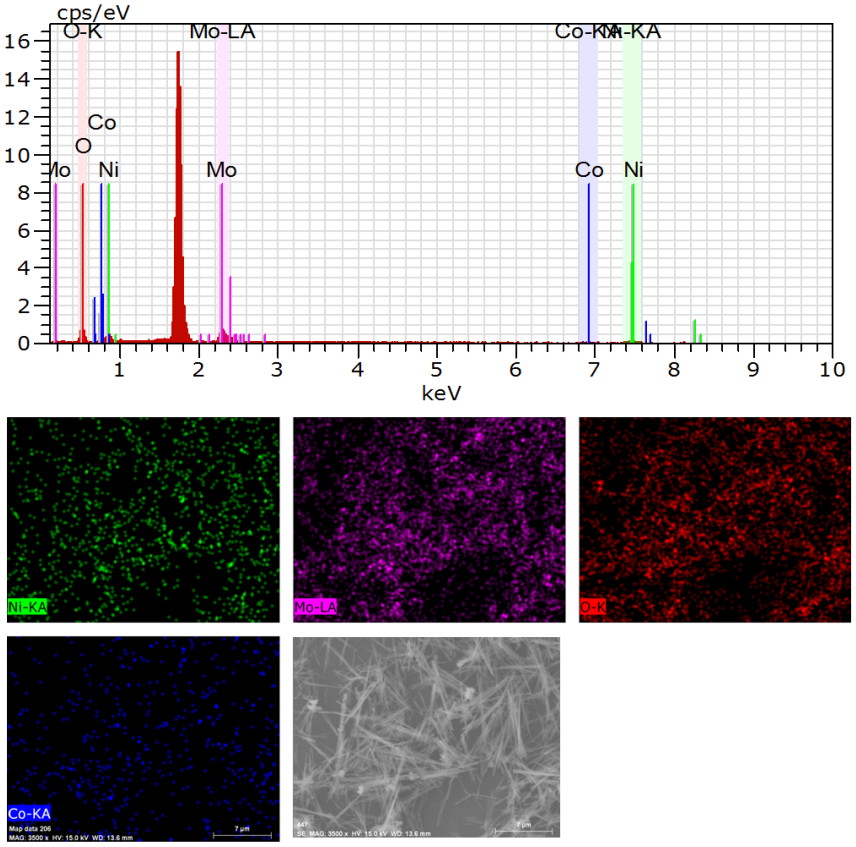

ESI Fig. 2

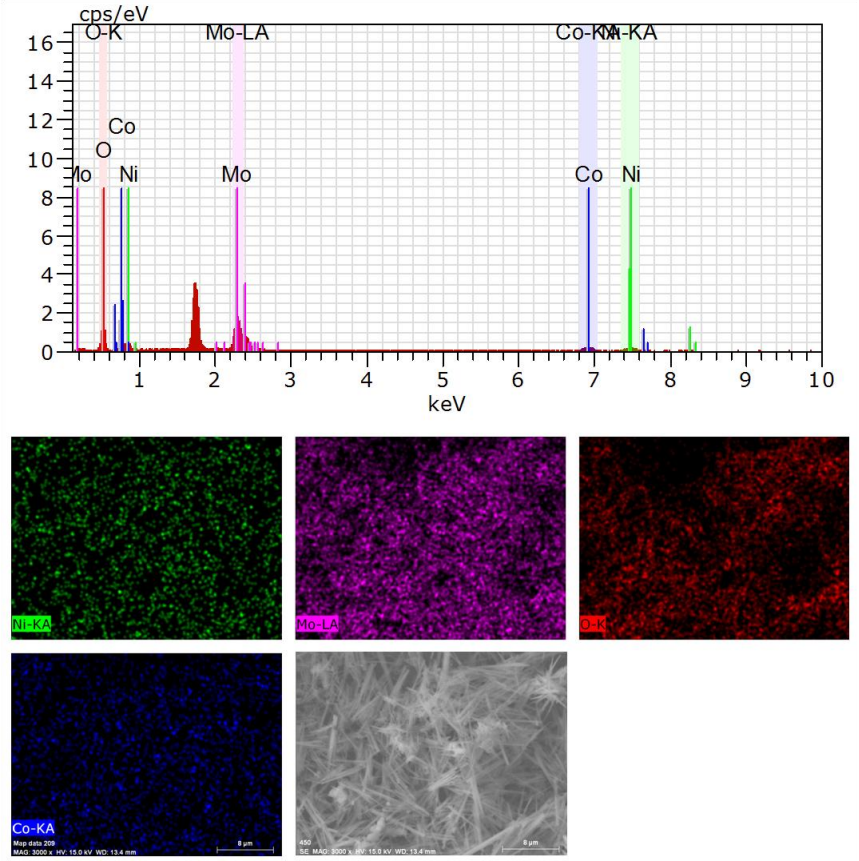

ESI Fig. 3

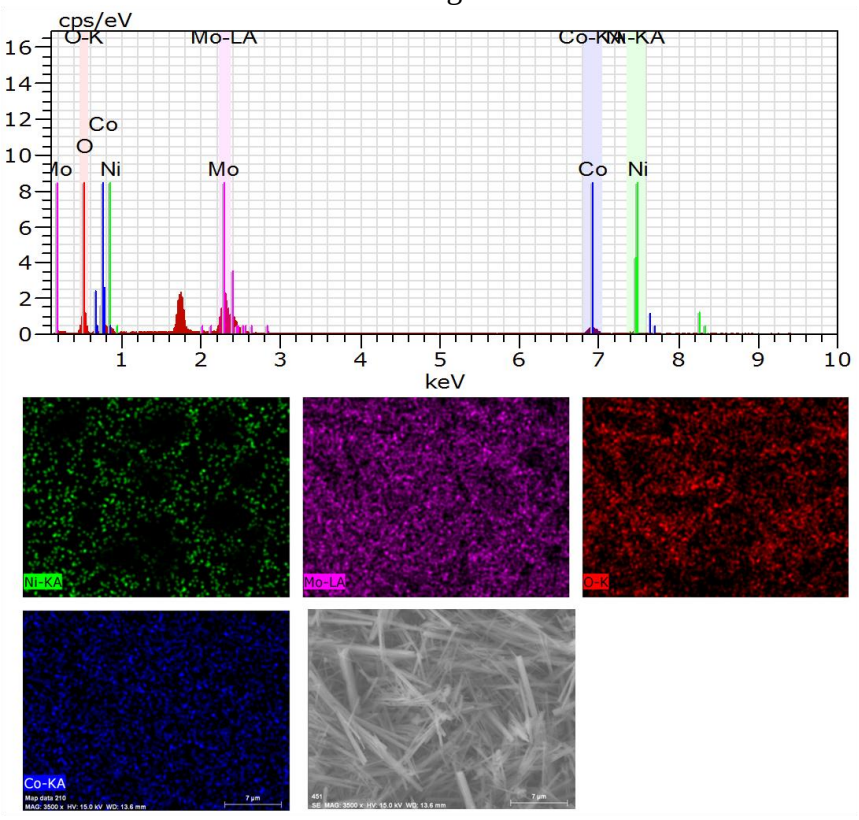

ESI Fig. 4

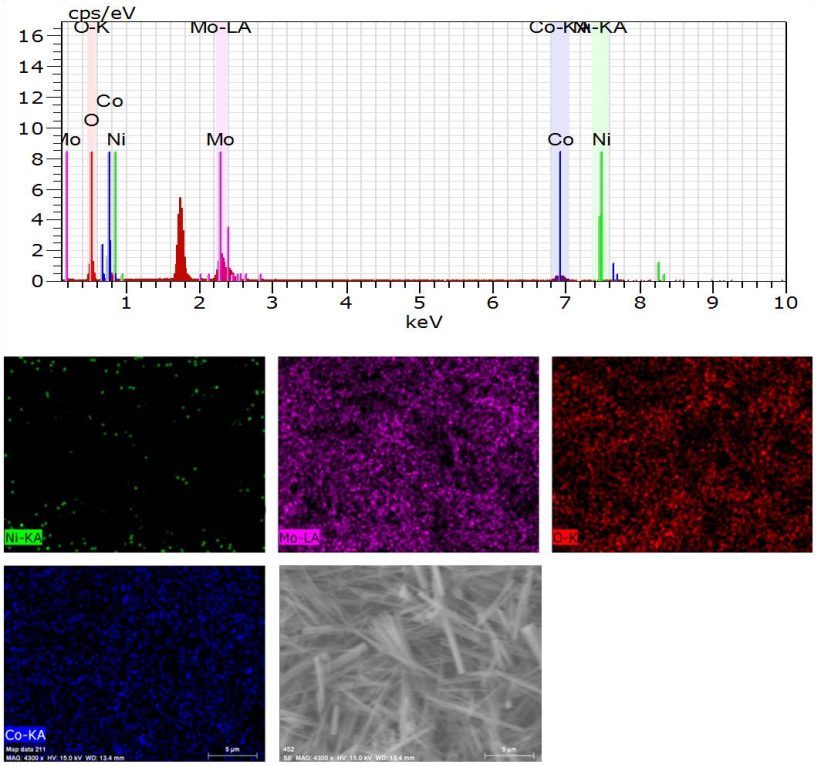

ESI Fig. 5